Eur. Phys. J. D **39**, 41–48 (2006)
DOI: 10.1140/epjd/e2006-00069-3

THE EUROPEAN PHYSICAL JOURNAL D

The structure of 55-atom Cu–Au bimetallic clusters: Monte Carlo study

D. Cheng, S. Huang[a], and W. Wang[b]

Division of Molecular and Materials Simulation, Key Lab for Nanomaterials, Ministry of Education, Beijing University of Chemical Technology, Beijing 100029, P.R. China

Received 21 October 2005 / Received in final form 18 January 2006
Published online 4 April 2006 –

Abstract. We have investigated segregation phenomena in Cu–Au bimetallic clusters with decahedral structures at 100 K and 300 K, based on the second-moment approximation of the tight-binding (TB-SMA) potentials by using Monte Carlo method. The simulation results indicate that there are three regions (split, three-shell onion-like and core-shell region) at 100 K and two regions (split and core-shell) at 300 K with the structure of decahedral clusters, as the chemical potential difference $\Delta\mu$ changes. It is found that the structure of decahedral clusters undergoes a division into smaller clusters in the split region. In the core-shell structure, Au atoms are enriched in surface and Cu atoms occupy the core of the clusters because of the different surface energy of Cu and Au. The Au atoms are enriched in the surface shell, and the Cu atoms are in the middle shell, while a single Au atom is located in the center to form the three-shell onion-like structure. The structure and binding energy of smaller clusters after splitting are also discussed. The Au atoms generally lie on the surface of the smaller clusters after splitting.

PACS. 36.40.-c Atomic and molecular clusters – 61.46.-w Nanoscale materials

1 Introduction

Bimetallic clusters are an active research field for the improvement of the catalytic properties for metal clusters [1–3]. The major interest in bimetallic clusters is that their properties depend not only on size but also on composition and atomic ordering [4]. Cu–Au alloy has received a great deal of recent attention, because its bulk properties and structures have been well established [5]. Surface segregation phenomena and order-disorder transition of Cu–Au nanoalloy have been extensively and intensively studied both in experiment [6–8] and theory [9–12]. Among the recent researches, Padovani et al. prepared Cu–Au bimetallic clusters on silica films [13]. Kim and coworkers prepared Cu–Au bimetallic clusters with the average size of 3.0 nm in chloroform [14]. Maurizio and coworkers studied the short-range order and crystalline structure of Cu–Au bimetallic clusters by EXAFS and GIXRD [15]. They found that the nearest neighbor distances of Au–Au, Cu–Cu and Cu–Au are different from the chemically disordered solid solution of Cu–Au alloys. Meanwhile, Van Hoof and coworkers studied the order-disorder phase transition and surface gold segregation phenomena by Monte Carlo simulations [16]. Rodríguez-López and coworkers simulated Cu–Au bimetallic clusters with different atomic structures using classical molecular dynamics simulations [17]. They found the Au-shell/Cu-core structure in the cluster at high temperatures, just before the melting point. Darby and coworkers investigated Cu–Au bimetallic clusters using a genetic algorithm with up to 56 atoms [18]. It is reported that the smaller Cu atom prefers to occupy the center of the cluster in doping gold clusters with a single Cu atom. Also, their calculated results indicate that Au atoms generally lie on the surface, while Cu atoms are encapsulated in the decahedral alloy clusters. Wilson and Johnson also found the phenomenon that Au atoms sit on the surface and Cu atoms in the core on the highly symmetric icosahedral and cuboctahedral Cu–Au bimetallic clusters by energy calculations [19].

Atomic ordering (segregation or mixing) is essential for bimetallic clusters, because the chemical and physical properties of bimetallic clusters can be tuned. In a preliminary study of bimetallic clusters, it is found that the core-shell structure both in experiment [20–22] and theory [23–33]. In addition, the three-shell onion-like structure was predicted by using theoretical methods [29–33]. These structures can present unusual catalytic properties and provide a basis for an economical design of nanoalloy catalysts by arranging the atoms of precious catalysts predominately on the outer surfaces of the clusters in terms of the surface segregation process [32].

[a] e-mail: huangsp@mail.buct.edu.cn
[b] e-mail: wangwc@mail.buct.edu.cn

Segregation is a spontaneous process, in which the Gibbs free energy decreases. Consequently, the equilibrium composition corresponds to the minimum of the Gibbs free energy [34]. A Monte Carlo (MC) method, based on the Metropolis algorithm, has been successfully used to simulate the segregation processes in the nanosystems [34–40], including the surface segregation of bimetallic clusters [16,32,41–44].

Aim of this work is at understanding the atomic ordering and structures for Cu–Au bimetallic clusters. In order to bring this problem to a clear description, we focus on the Cu–Au bimetallic clusters of 55 atoms with decahedral structure by using the Monte Carlo (MC) simulation method first. Then, we discuss the structure characteristics of Au_xCu_y clusters at different compositions.

2 Computational details

2.1 Initial cluster configurations

In general, the initial geometry of decahedral clusters possesses fivefold symmetry, and fragments of the face-centered cubic (fcc) lattice. In this work, we took the initial structure of a cluster from the work of Turner et al. [45]. Before starting the Monte Carlo runs, a relatively short steepest-descent minimization was performed to relax the lattice in the initial configuration, which was based on the embedded atom method (EAM) potential [46].

2.2 Potential models and parameters

In the Monte Carlo runs, we adopted the second-moment approximation of the tight-binding (TB-SMA) potential scheme for the description of the interaction between atoms. Within the second moment approximation of the tight-binding (TB-SMA) potential [47], the total energy of a system is expressed as

$$E_c = \sum_i \left(E_R^i + E_B^i\right) \tag{1}$$

where E_B^i and E_R^i are the band and Born-Mayer ion-ion repulsions term, respectively. The both terms can be written for an atom i as

$$E_R^i = \sum_j A_{\alpha\beta} e^{-P_{\alpha\beta}\left(r_{ij}/r_0^{\alpha\beta}-1\right)},$$

$$E_B^i = -\left\{\sum_j \xi_{\alpha\beta}^2 e^{-2q_{\alpha\beta}\left(r_{ij}/r_0^{\alpha\beta}-1\right)}\right\}^{1/2} \tag{2}$$

where A, ξ, p, q and r_0 of the TB-SMA scheme are obtained by fitting to the experimental values of the cohesive energy, lattice parameters (by a constraint on the atomic volume), and independent elastic constants for the reference crystal structure at $T = 0$ K. In addition, $r_0 = a_0/\sqrt{2}$ (a_0 is the independent lattice constant for each pure system and for alloys), and r_{ij} is the distance between atoms i and j in the cluster.

Table 1. Parameters of the TB-SMA potential for Cu–Au bimetallic clusters.

	A (eV)	ξ(eV)	p	q	a_0 (Å)
Cu–Cu	0.0855	1.224	10.960	2.278	3.615
Au–Au	0.2061	1.790	10.229	4.036	4.079
Cu–Au	0.1539	1.5605	11.05	3.0475	3.615

For Au_xCu_y bimetallic clusters, the parameters are of different values for each of the different interactions (Au–Au, Cu–Cu, and Cu–Au). The potential models calculated for pure elements (Au–Au and Cu–Cu) were derived by fitting to the pure metals and remained unchanged in the simulation. The Cu–Au potential parameters were obtained by fitting to the mechanical and thermodynamic properties of the bulk Cu_3Au. The potential parameters were developed by Cleri and Rosato [47], which were employed for the theoretical study of Cu–Au bimetallic clusters with satisfactory results [18,19].

All the potential parameters used in this work are listed in Table 1.

From the total cluster potential energy, V_{clus}, the average binding energy, E_b, for an N-atom cluster is defined as the positive quantity:

$$E_b = \frac{-V_{clus}}{N}. \tag{3}$$

2.3 Monte Carlo simulations

In Monte Carlo simulations, the segregation processes are simulated by changing the chemical type of the atoms and slightly displacing the atoms from their original positions [34]. Two approaches can be used: the canonical ensemble and the grand canonical ensemble. In the canonical ensemble simulation, two different atoms picked randomly are interchanged. In contrast, the grand canonical ensemble simulation proceeds by picking an atom and then changing its type. The equilibrium composition is gained by maintaining the correct chemical potential difference $\Delta\mu$ ($\Delta\mu = \mu_{\mathrm{Cu}} - \mu_{\mathrm{Au}}$) between the two species.

In our study of the Cu–Au bimetallic clusters, grand canonical Monte Carlo (MC) simulations were performed [35,36], in which the total number of atoms ($N = N_{\mathrm{Cu}} + N_{\mathrm{Au}}$), temperature ($T$) and chemical potential difference ($\Delta\mu = \mu_{\mathrm{Cu}} - \mu_{\mathrm{Au}}$) between the two species were fixed. The algorithm allowed to vary N_{Cu} and N_{Au}. The chemical composition at a given temperature was therefore obtained by performing the MC simulation at a fixed value of chemical potential difference $\Delta\mu$ between the two species in the cluster. The volume of the system may or may not be in fluctuations. It is noted that the segregation can be well predicted with this method at surfaces [34,37–39] and interfaces [40]. Meanwhile, the similar algorithm proved to be successful in the study of the surface segregation of bimetallic clusters [16,44].

The probability of state X_i in the grand canonical ensemble can be expressed as [36]

$$f(X_i) = P_i \sim \left(V/\Lambda_A^3\right)^{N_A} \left(V/\Lambda_B^3\right)^{N_B} \times \exp\left[-(E_x - N_A\mu_A - N_B\mu_B)/k_BT\right] \quad (4)$$

where V, E_x, T and k_B represent the volume of the system, the energy of configuration X, the temperature and the Boltzmann constant, respectively. N_A and N_B stand for the number of A and B atoms, respectively. Λ_A, Λ_B, μ_A and μ_B are the thermal De Broglie wavelength and the chemical potential of component A and B, respectively.

The Monte Carlo codes used here were written by us, and tested by the experiment [6] and other Monte Carlo simulation results [9]. The codes can be used to simulate the surface segregation of binary alloys and bimetallic clusters. For the bimetallic clusters, the MC simulation method includes two types of trials:

(1) displacement of each atom from its original position in a random direction, which corresponds to the relaxation and vibration movements. The new configuration is retained with a probability P_{XY} (from state X to state Y), given by

$$P_{XY} = \exp\left[-\Delta E/k_BT\right]; \quad (5)$$

(2) random selection of the chemical type of an atom, corresponding to the fixed chemical potential difference $\Delta\mu$ between the two species and allowing the system to reach compositional equilibrium. The relative probability P_{XY} (from state X to state Y), where an A atom is replaced by a B atom, is given by [34]

$$P_{XY} = \left(\Lambda_A^3/\Lambda_B^3\right) \exp\left[-\left(\Delta E + \Delta\mu\right)/k_BT\right]. \quad (6)$$

Here, if $P_{XY} > 1$, the new configuration is always retained, while if $P_{XY} \leq 1$, the new configuration is accepted with the probability P_{XY}.

In our MC simulations, 20000 steps were run for each atom. The first 10000 steps/per-atom were used for reaching the equilibrium, where the fluctuation of the total energy of the system was less than 0.2%, and the last 10000 steps/per-atom for an average of the structural properties.

2.4 Pair correlation function

The pair correlation function is the probability of an atom occurring in the spherical shell between r and $r + dr$. We define $g_{cm}(r)$ as the pair correlation function around the centre of mass for the bimetallic clusters. The $g_{cm}(r)$ is calculated from trajectories of the MC simulation after equilibrium, given by

$$g_{cm}(r) = \frac{V}{N^2} \left\langle \sum_{i=1}^{n} \delta(\vec{r} - \vec{r}_i - \vec{r}_{cm}) \right\rangle \quad (7)$$

where N is the total atom number of whole bimetallic cluster (55 for this work), V is the volume of the bimetallic cluster, n is the atom number counted, and $\vec{r}_{cm}$ is the coordinates of the centre of mass at each MC step.

In this work, we define $g^*_{cm}(r) = g_{cm}(r)/(V/N^2)$, and then the reduced pair correlation function $g^*_{cm}(r)$ is given by

$$g^*_{cm}(r) = \left\langle \sum_{i=1}^{n} \delta(\vec{r} - \vec{r}_i - \vec{r}_{cm}) \right\rangle. \quad (8)$$

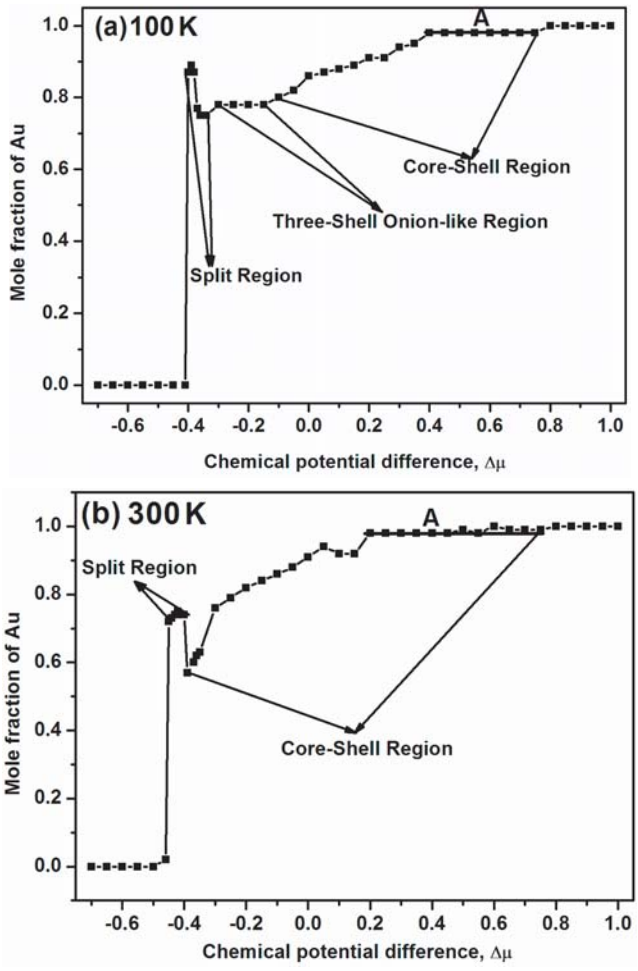

Fig. 1. The simulation equilibrium mole fraction of Au in the cluster verses the chemical potential difference $\Delta\mu$ ($\Delta\mu = \mu_{\mathrm{Cu}} - \mu_{\mathrm{Au}}$). (a) 100 K. (b) 300 K. The symbol "A" denotes the core-shell structure of Cu_1Au_{54}.

3 Results and discussion

Figure 1 shows the Au mole fraction changing with the chemical potential difference $\Delta\mu$ ($\Delta\mu = \mu_{\mathrm{Cu}} - \mu_{\mathrm{Au}}$) for the clusters with the initial geometry of decahedron at 100 K and 300 K, respectively. It is found in Figure 1 that as the chemical potential difference $\Delta\mu$ changes, some distinct characteristics of the structures of the bimetallic clusters are observed, such as the core-shell and three-shell onion-like structures. It is also found that the Cu atoms

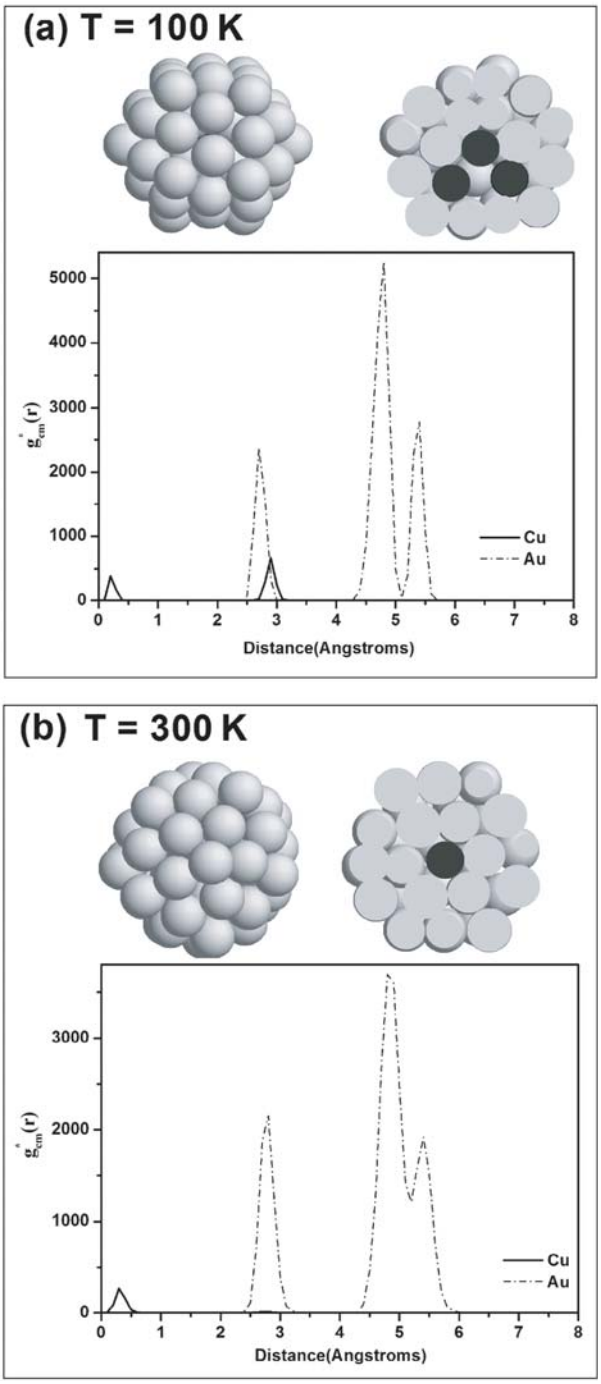

Fig. 2. The snapshots (dark gray atoms, Cu; light gray atoms, Au) and reduced pair correlation functions (Cu, solid line; Au, dash-dot line) of clusters at $\Delta\mu = 0.3$ eV. (a) Cu_3Au_{52} with the core-shell structure at 100 K. (b) Cu_1Au_{54} with the core-shell structure at 300 K.

prefer to occupy the cores of the clusters and Au atoms generally lie on the surfaces due to the different surface energies (see Fig. 2), which is in good agreement with the results from the genetic algorithm [18]. Meanwhile, a recent study about the optimization of Cu–Au clusters within the Gupta model explains that the tendency to surface segregation of Au in Cu–Au clusters is due to the interplay of size mismatch and bond-order/bond-length correlation [48]. The symbol "A" in Figure 1 represents the occurrence of core-shell structure of Cu_1Au_{54}, where a smaller Cu atom occupies the center of the cluster. It is also consistent with the results from the genetic algorithm [18] and energy calculation [19].

As is seen in Figure 1a, the Au mole fraction of the cluster appears a drastic jump from 0.00 to 0.87 in the range of $\Delta\mu \sim -0.40$ to -0.34 eV, which implies the rearrangement of Cu and Au atoms in the cluster at 100 K. Based on the observations in Figure 1a, we can define three regions at 100 K: (1) $\Delta\mu$ is from -0.40 to -0.34 eV, the split region. (2) $\Delta\mu$ is from -0.30 to -0.15 eV, the three-shell onion-like region. Note that the three-shell onion-like structure has also been reported recently in the investigation on the bimetallic clusters, for example, Pd–Pt [30], Pt–Ni [32], and other clusters [29,31,33]. (3) $\Delta\mu$ is from -0.10 to 0.75 eV, the core-shell region. Such a core-shell structure has been observed for some bimetallic clusters [18–33].

The Au mole fraction exhibits a great jump at $\Delta\mu = -0.45 \sim -0.40$ eV at 300 K, shown in Figure 1b. It is found in Figure 1b that there are two regions for a Cu–Au bimetallic cluster at 300 K, as the chemical potential difference $\Delta\mu$ changes. One is the split region in the range of $\Delta\mu = -0.45 \sim -0.40$ eV, and the other is the core-shell region.

In order to analyze the core-shell and three-shell onion-like structures in detail, the reduced pair correlation function and average binding energy were calculated. In the core-shell structure, a core of Cu atoms is surrounded by a thin shell of Au atoms, which presents the tendency to segregate to the surface due to the different surface energies. Figure 2 shows the snapshots and reduced pair correlation functions of the core-shell structures with $\Delta\mu \sim 0.3$ eV at 100 K and 300 K, respectively. The reduced pair correlation functions indicate that the Cu atoms are in the core and Au atoms are on the surface layer. The results are in good agreement with that of the genetic algorithm for the lowest energy structure of Cu–Au clusters [18]. When $\Delta\mu = 0.3$ eV, the cluster embodies different structures: the decahedron-like (decahedron with flaws) structure at 100 K (see Fig. 2a) and the icosahedron-like (icosahedron with flaws) structure at 300 K (see Fig. 2b). It means that the decahedral structure can be transformed into the icosahedron-like structure at 300 K, which is consistent with the results of Baletto et al. [49]. The average binding energies with subshell labeling {Cu–Au–Au} (the string from left to right means a central Cu atom, the Au atoms in the first shell and the second shell) are 3.436 eV and 3.396 eV with $\Delta\mu \sim 0.4$ eV at 100 K and 300 K, respectively, which is in agreement with the average binding energy in the previous study [19].

For the three-shell onion-like structure, Cu atoms accumulate in the layer just below the surface, thus forming an intermediate shell {Au–Cu–Au} with the three-shell onion-like structure. The three-shell onion-like structure was found in the 55-atom Pd–Pt bimetallic cluster by using the genetic algorithm global optimization based on

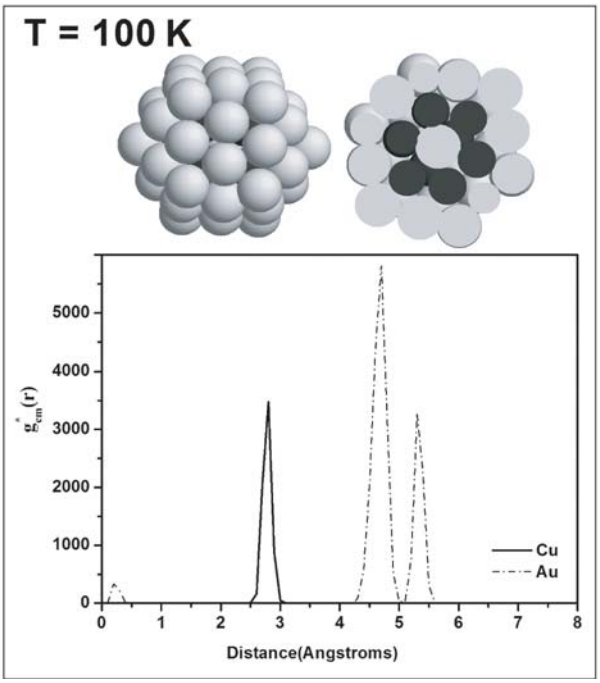

Fig. 3. The snapshots (dark gray atoms, Cu; light gray atoms, Au) and reduced pair correlation functions (Cu, solid line; Au, dash-dot line) of the cluster with the structure of three-shell onion-like at 100 K when $\Delta\mu = -0.3$ eV.

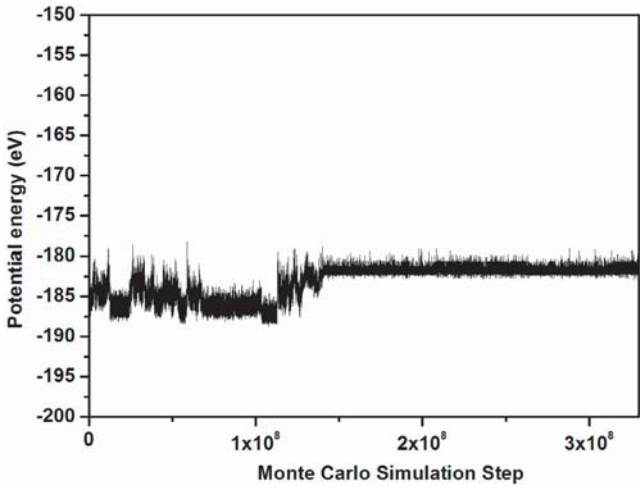

Fig. 4. The potential energy as a function of MC steps for the cluster at 100 K when $\Delta\mu$ is –0.36 eV.

the second-moment approximation of the tight-binding (TB-SMA) model [30], and Pt–Ni catalyst clusters with MC simulation from the modified embedded atom method (MEAM) [32]. In our simulations, it is also found that there is a three-shell onion-like structure in Cu–Au clusters with $\Delta\mu = -0.3$ eV at 100 K (see Fig. 3). Snapshots and the reduced pair correlation functions show clearly that a single Au atom pushes away the Cu atoms to occupy the central site, and the Cu atoms form an intermediate shell, completely covering the central single Au atom. Meanwhile, the other Au atoms accumulate on the surface layer, covering the Cu atoms shell. We also calculated the average binding energies with the three-shell onion-like structure, which is 3.428 eV at 100 K when $\Delta\mu = -0.3$ eV.

In order to understand clearly the split phenomenon of 55-atom Cu–Au bimetallic clusters, $\Delta\mu$ values were carefully selected from -0.34 to -0.40 eV at 100 K and from -0.40 to -0.45 eV at 300 K. MC simulation steps were set to 3.30×10^8 to guarantee system equilibration. Figure 4 represents the potential energy of the cluster as a function of MC steps for the 55-atom Cu–Au bimetallic clusters at $\Delta\mu = -0.36$ eV and 100 K. It is found that the fluctuation of the potential energy of the cluster becomes reasonable after 1.50×10^8 steps, which indicates that the simulation system reached equilibration. In the splitting region, the 55-atom Cu–Au bimetallic cluster splits into three small clusters while all the small clusters are of $\Delta\mu = -0.36$ eV at 100 K. Their chemical formulae can be expressed as Cu_1Au_{12}, Cu_2Au_{14} and Cu_4Au_{22}. The Au mole fractions of the three small clusters are 0.923, 0.875 and 0.846, respectively.

The structures after splitting are shown in Figure 5 at 100 K with $\Delta\mu = -0.34 \sim -0.40$ eV and their potential energies are listed in Table 2. The 55-atom Cu–Au bimetallic cluster is decomposed into two, three or four clusters as the chemical potential difference $\Delta\mu$ changes. It is found that Cu atoms get together in the center of the clusters and Au atoms generally lie on the surfaces to increase the binding energy of clusters, which is in good agreement with the results from the genetic algorithm [18]. The results indicate that some lower energy clusters, such as Au_7, Cu_1Au_{12}, Cu_1Au_{13} and Cu_2Au_{17}, can be obtained by splitting from the 55-atom Cu–Au bimetallic cluster at 100 K.

When $\Delta\mu$ is -0.37 eV at 100 K, the 55-atom decahedral cluster is decomposed into three small clusters of the atom numbers of 13, 19 and 23 (see the third row in Fig. 5). Their chemical formulae can be expressed as Cu_1Au_{12}, Cu_2Au_{17} and Cu_3Au_{20}. The structure of Cu_1Au_{12} consists of 12 Au atoms and a single Cu atom in the central site (see the fourth and fifth row in Fig. 5). It is noticed that this core-shell structure is the minimum energy structure of Cu_1Au_{12}, which is reported by molecular dynamics simulations [50]. The Cu_2Au_{17} cluster here contains two 13-atom core-shell structures with a coplanar plane, and each Cu atom in the centre of the 13-atom core-shell structure, as is shown in the third row of Figure 5 (also see the fifth row). The Cu_3Au_{20} cluster can be seen as integration of the three 13-atom core-shell clusters in the third row of Figure 5. The 55-atom cluster would not keep its shape, and change into four small clusters when $\Delta\mu = -0.38$ eV at 100 K. The fourth row in Figure 5 shows the structure of the four smaller clusters. Two of their chemical formulae are Cu_1Au_{13}, and the others can be expressed as Au_7 and Cu_2Au_{18}, respectively. The structure of Cu_1Au_{13} shown in the fourth row of Figure 5 (also see the sixth row in Fig. 5) consists of 13 Au atoms and a single Cu atom in the central site. Interestingly,

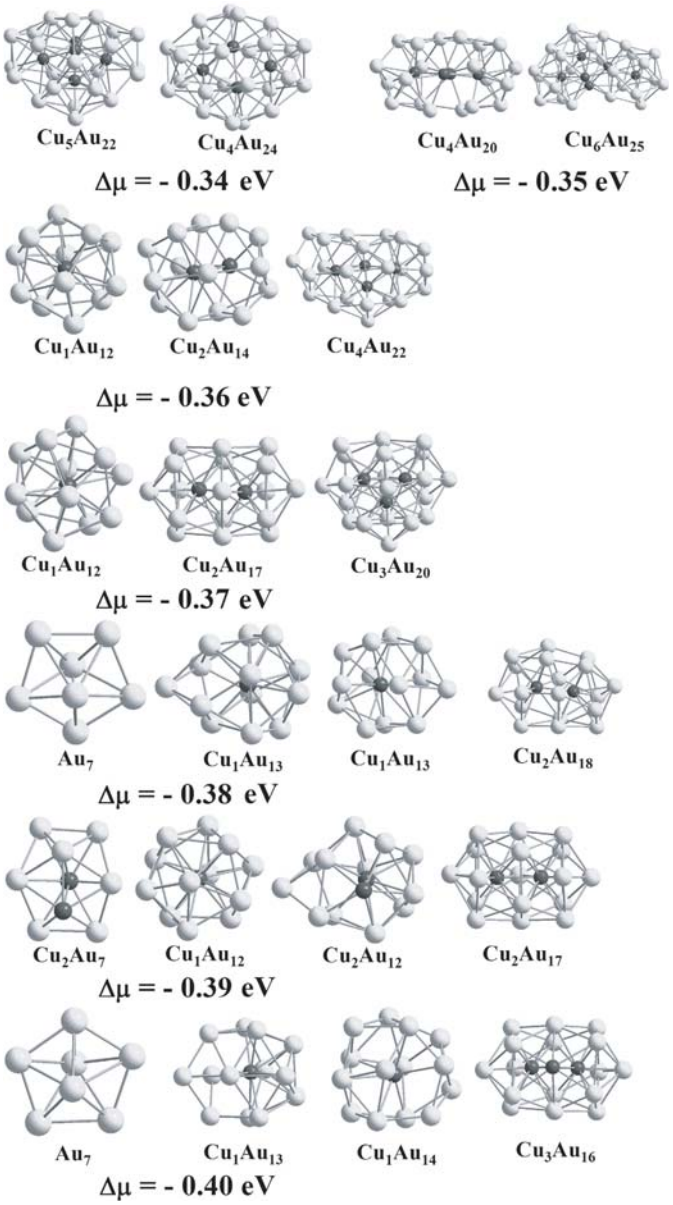

Fig. 5. The structure of small clusters in the split region at 100 K with $\Delta\mu = -0.34 \sim -0.40$ eV (dark gray atoms, Cu; light gray atoms, Au).

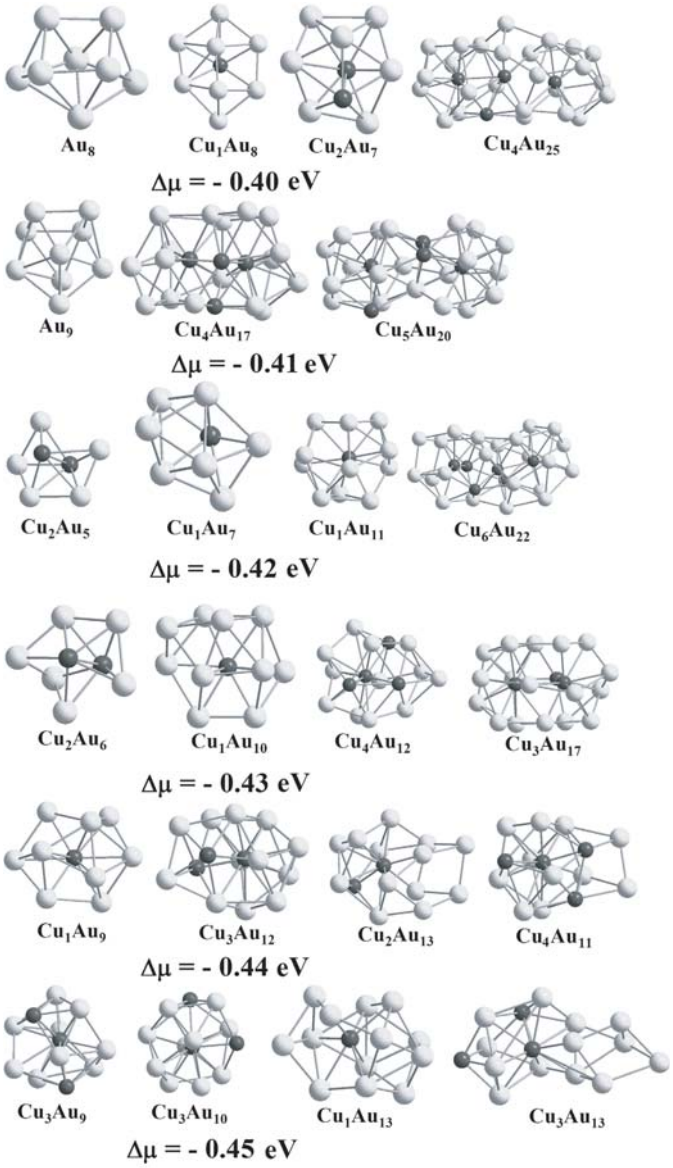

Fig. 6. The structure of small clusters in the split region at 300 K with $\Delta\mu = -0.40 \sim -0.45$ eV (dark gray atoms, Cu; light gray atoms, Au).

a core-shell structure Cu_1Au_{13} is also reported based on the genetic algorithm calculation [18]. The Au_7 cluster possesses the decahedral structure (see the fourth and sixth row in Fig. 5). The Cu_2Au_{18} cluster is also of the coplanarity of two 13-atom core-shell structures, and a Cu atom is located in the centre of the 13-atom core-shell structure, as is shown in the fourth row of Figure 5.

Figure 6 shows the structures of small clusters after splitting at 300 K with $\Delta\mu = -0.40 \sim -0.45$ eV, and the potential energies are also listed in Table 2. By comparing the potential energies of the small clusters of the same atom number at 300 K with 100 K, it is found that the potential energies at 100 K are lower (see Tab. 2), when the atomic number is the same. Some small Cu_xAu_y cluster isomers, with a fixed number of atoms ($N = x + y$, x and y represent the number of Cu and Au, respectively) and different composition (x/y ratio), are shown in Figure 6. For example, Au_8, Cu_1Au_7 and Cu_2Au_6 (see the first, third and fourth row in Fig. 6) , as well as Cu_1Au_8, Cu_2Au_7 and Au_9 (see the first and second row in Fig. 6) are of the same total number of atoms. It implies that bimetallic clusters are more complex than pure metal clusters because of the different types of atoms and geometrical isomers.

Figure 7 shows a comparison of the average binding energies at 100 K and 300 K for small clusters after splitting. For the small clusters at 100 K, there exist pronounced

Table 2. The potential energy, depending on the chemical potential difference$\Delta\mu$, for smaller Cu–Au bimetallic clusters with the total number of atom (N) after splitting in the split region at 100 K and 300 K.

100 K				300 K			
N	Composition	$\Delta\mu$(eV)	energy(eV)	N	Composition	$\Delta\mu$(eV)	energy(eV)
7	Au_7	–0.38	–21.8014	7	Cu_2Au_5	–0.42	–19.6789
7	Au_7	–0.4	–21.8716	8	Cu_2Au_6	–0.43	–23.3364
9	Cu_2Au_7	–0.39	–27.3459	8	Cu_1Au_7	–0.42	–24.2168
13	Cu_1Au_{12}	–0.37	–42.6892	8	Au_8	–0.4	–24.8285
13	Cu_1Au_{12}	–0.39	–42.8531	9	Cu_2Au_7	–0.4	–26.9671
13	Cu_1Au_{12}	–0.36	–42.9293	9	Cu_1Au_8	–0.4	–27.3451
14	Cu_2Au_{12}	–0.39	–44.9843	9	Au_9	–0.41	–28.2171
14	Cu_1Au_{13}	–0.38	–45.6982	10	Cu_1Au_9	–0.44	–30.9729
14	Cu_1Au_{13}	–0.4	–45.7689	11	Cu_1Au_{10}	–0.43	–34.1427
14	Cu_1Au_{13}	–0.38	–45.904	12	Cu_3Au_9	–0.45	–36.802
15	Cu_1Au_{14}	–0.4	–48.7892	12	Cu_1Au_{11}	–0.42	–38.4241
16	Cu_2Au_{14}	–0.36	–51.4796	13	Cu_3Au_{10}	–0.45	–40.5018
19	Cu_3Au_{16}	–0.4	–62.7437	14	Cu_1Au_{13}	–0.45	–44.4011
19	Cu_2Au_{17}	–0.37	–63.4571	15	Cu_4Au_{11}	–0.44	–46.7434
19	Cu_2Au_{17}	–0.39	–63.5418	15	Cu_2Au_{13}	–0.44	–47.3207
20	Cu_2Au_{18}	–0.38	–66.5105	15	Cu_3Au_{12}	–0.44	–47.6429
23	Cu_3Au_{20}	–0.37	–77.2666	16	Cu_3Au_{13}	–0.45	–48.3399
24	Cu_4Au_{20}	–0.35	–78.9764	16	Cu_4Au_{12}	–0.43	–49.774
26	Cu_4Au_{22}	–0.36	–86.5889	20	Cu_3Au_{17}	–0.43	–64.8874
27	Cu_5Au_{22}	–0.34	–90.5763	21	Cu_4Au_{17}	–0.41	–67.3874
28	Cu_4Au_{24}	–0.34	–94.0997	25	Cu_5Au_{20}	–0.41	–80.8856
31	Cu_6Au_{25}	–0.35	–103.904	28	Cu_6Au_{22}	–0.42	–90.1825
				29	Cu_4Au_{25}	–0.4	–94.8079

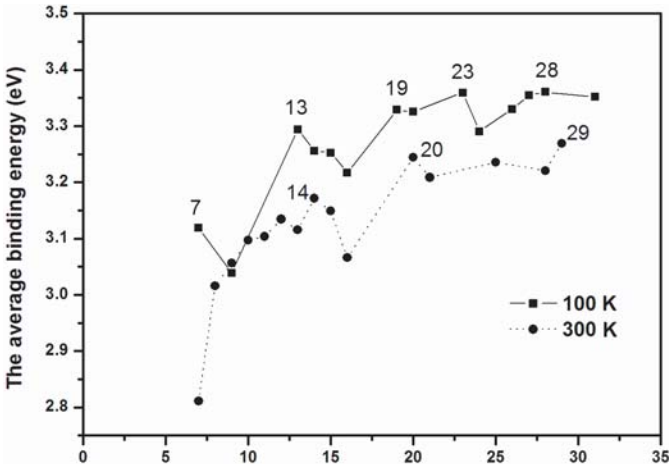

Fig. 7. The average binding energy of the small clusters in the split region at 100 K (solid line with square point) and 300 K (dotted line with round point).

peaks with the size N = 7, 13, 19, 23 and 28. This observation coincides with the results of Rossi et al. [51], where a set of stable clusters of 13, 19 and 23 atoms, corresponding to the first three core-shell polyicosahedra structures, are found for Ag–Cu and Ag–Ni clusters. In contrast, there are remarkable peaks at N = 14, 20 and 29 in our simulations at 300 K.

4 Conclusions

In this work, we focused on segregation of 55-atom Cu–Au bimetallic clusters, using the second-moment approximation of the tight-binding (TB-SMA) potentials and Monte Carlo method. The simulation results indicate that there are three regions with the structure of decahedral clusters at 100 K: the split region, three-shell onion-like region and core-shell region as the chemical potential difference $\Delta\mu$ changes. In contrast, only two regions, the split and core-shell region, exist at 300 K. In the three-shell onion-like structure, the Au atoms are enriched in the surface shell, and the Cu atoms are in the middle shell, while a single Au atom is located in the center to form the {Au–Cu–Au} structure. On the other hand, Au atoms are enriched in the surface shell covering the Cu atoms in the core-shell structure. It is found in the split region that the decahedral clusters split into smaller clusters. Such smaller clusters hold Cu atoms in the core because of the different surface energy of Cu and Au. It is noticed that there are pronounced peaks with the total atomic number N = 7, 13, 19, 23 and 28 at 100 K, which correspond to the structures of small clusters with symmetric geometries and greater stability. In contrast, there are remarkable peaks at N = 14, 20 and 29 at 300 K. In summary, the simulation results here suggest a possibility to control atomic order in preparation of catalyst clusters.

This work is supported by the National Natural Science Foundation of China (No. 20476004 and 20236010), and

the National Basic Research Program of China (Grant No. G2003CB615807).

References

1. J.H. Sinfelt, *Bimetallic catalysts: discoveries, concepts, and applications* (Wiley, New York, 1983)
2. N. Toshima, T. Yonezawa, New J. Chem. 1179 (1998)
3. S.P. Huang, P.B. Balbuena, J. Phys. Chem. B. **106**, 7225 (2002)
4. F. Baletto, R. Ferrando, Rev. Mod. Phys. **77**, 371 (2005)
5. M.A. Vasiliev, J. Phys. D: Appl. Phys. **30**, 3037 (1997)
6. H. Reichert, H. Dosch, Surf. Sci. **345**, 27 (1996)
7. S. Mróz, A. Mróz, Vacuum **48**, 369 (1997)
8. E. Taglauer, R. Beikler, Vacuum **73**, 9 (2004)
9. M.A. Hoffmann, P. Wynblatt, Surf. Sci. **236**, 369 (1990)
10. M. Hou, M.El. Azzaoui, Surf. Sci. **380**, 210 (1997)
11. A. Maidou, H.M. Polatoglou, Phys. Rev. B **60**, 9145 (1999)
12. B. Good, G.H. Bozzolo, P.B. Abel, Surf. Sci. **454–456**, 602 (2000)
13. S. Padovani, F. D'Acapito, E. Cattaruzza, A. De Lorenzi, F. Gonella, G. Mattei, C. Maurizio, P. Mazzoldi, M. Montagna, S. Ronchin, C. Tosello, M. Ferrari, Eur. Phys. J. B **25**, 11 (2002)
14. M.-J. Kim, H.-J. Na, K.C. Lee, E.A. Yoo, M.Y. Lee, J. Mater. Chem. **13**, 1789 (2003)
15. C. Maurizio, G. Mattei, P. Mazzoldi, S. Padovani, E. Cattaruzza, F. Gonelia, F. D'Acapito, F. Zontone, Nucl. Instrum. Meth. B **200**, 178 (2003)
16. T.V. Hoof, M. Hou, Appl. Surf. Sci. **226**, 94 (2004)
17. J.L. Rodríguez-López, J.M. Montejano-Carrizales, M. José-Yacamán, Appl. Surf. Sci. **219**, 56 (2003)
18. S. Darby, T.V. Mortimer-Jones, R.L. Johnson, C. Roberts, J. Chem. Phys. **116**, 1536 (2002)
19. N.T. Wilson, R.L. Johnson, J. Mater. Chem. **12**, 2913 (2002)
20. N. Toshima, M. Harada, T. Yonezawa, K. Kushihashi, K. Asakura, J. Phys. Chem. **95**, 7448 (1991)
21. N. Toshima, M. Harada, Y. Yamazaki, K. Asakura, J. Phys. Chem. **96**, 9927 (1992)
22. R. Harpeness, A. Gedanken, Langmuir **20**, 3431 (2004)
23. J.M. Montejano-Carrizales, M.P. Iñiguez, J.A. Alonso, Phys. Rev. B **49**, 16649 (1994)
24. J. Jellinek, E.B. Krissinel, Chem. Phys. Lett. **258**, 283 (1996)
25. E.B. Krissinel, J. Jellinek, Chem. Phys. Lett. **272**, 301 (1997)
26. M. Strobel, K.-H. Heinig, W. Möller, Nucl. Instrum. Meth. B **148**, 104 (1999)
27. J. Guevara, A.M. Llois, F. Aguilera-Granja, J.M. Montejano-Carrizales, Physica B **354**, 300 (2004)
28. L.D. Lloyd, R.L. Johnston, S. Salhi, N.T. Wilson, J. Mater. Chem. **14**, 1691 (2004)
29. A. Mañanes, M.P. Iñiguez, M.J. López, J.A. Alonso, Phys. Rev. B **42**, 5000 (1990)
30. C. Massen, T.V. Mortimer-Jones, R.L. Johnston, J. Chem. Soc., Dalton Trans. 4375 (2002)
31. F. Baletto, C. Mottet, R. Ferrando, Phys. Rev. Lett. **90**, 135504 (2003)
32. G.F. Wang, M.A. Van Hove, P.N. Ross, M.I. Baskes, J. Chem. Phys. **122**, 024706 (2005)
33. M.M. Mariscal, S.A. Dassie, E.P.M. Leiva, J. Chem. Phys. **123**, 184505 (2005)
34. P. Deurinck, C. Creemers, Surf. Sci. **419**, 62 (1998)
35. S.M. Foiles, Phys. Rev. B **32**, 7685 (1985)
36. *Surface Segregation Phenomena*, edited by S.M. Foiles, P.A. Dowben, A. Miller (CRC Press, Boca Raton, 1990)
37. H.Q. Deng, W.Y. Hu, X.L. Shu, L.H. Zhao, B.W. Zhang, Surf. Sci. **517**, 177 (2002)
38. H.Q. Deng, W.Y. Hu, X.L. Shu, B.W. Zhang, Surf. Sci. **543**, 95 (2003)
39. J.A. Brown, Y. Mishin, Phys. Rev. B **67**, 195414 (2003)
40. M. Hou, V.S. Kharlamov, E.E. Zhurkin, Phys. Rev. B **66**, 195408 (2002)
41. G.F. Wang, M.A. Van Hove, P.N. Ross, M.I. Baskes, J. Chem. Phys. **121**, 5410 (2004)
42. G.F. Wang, M.A. Van Hove, P.N. Ross, M.I. Baskes, J. Phys. Chem. B **109**, 11683 (2005)
43. G.F. Wang, M.A. Van Hove, P.N. Ross, M.I. Baskes, Prog. Surf. Sci. **79**, 28 (2005)
44. E.E. Zhurkin, M. Hou, J. Phys.: Condens. Matter **12**, 6735 (2000)
45. G.W. Turner, R.L. Johnston, N.T. Wilson, J. Chem. Phys. **112**, 4773 (2000)
46. M.A. Meineke, C.F. Vardeman II, L. Teng, C.J. Fennell, J.D. Gezelter, J. Comput. Chem. **26**, 252 (2005)
47. F. Cleri, V. Rosato, Phys. Rev. B **48**, 22 (1993)
48. A. Rapallo, G. Rossi, R. Ferrando, A. Fortunelli, B.C. Curley, L.D. Lloyd, G.M. Tarbuck, R.L. Johnson, J. Chem. Phys. **122**, 194308 (2005)
49. F. Baletto, J.P.K. Doye, R. Ferrando, C. Mottet, Surf. Sci. **532–535**, 898 (2003)
50. M.J. López, P.A. Marcos, J.A. Alonso, J. Chem. Phys. **104**, 1056 (1996)
51. G. Rossi, A. Rapallo, C. Mottet, A. Fortunelli, F. Baletto, R. Ferrando, Phys. Rev. Lett. **93**, 105503 (2004)